nature geoscience
SUPPLEMENTARY INFORMATION
DOI: 10.1038/NGEO2833

In the format provided by the authors and unedited.

Regional energy budget control of the intertropical convergence zone and application to mid-Holocene rainfall

WILLIAM R. BOOS*

Department of Geology and Geophysics
Yale University, New Haven, Connecticut, 06511, USA

ROBERT L. KORTY

Department of Atmospheric Sciences
Texas A&M University, College Station, Texas, 77843, USA

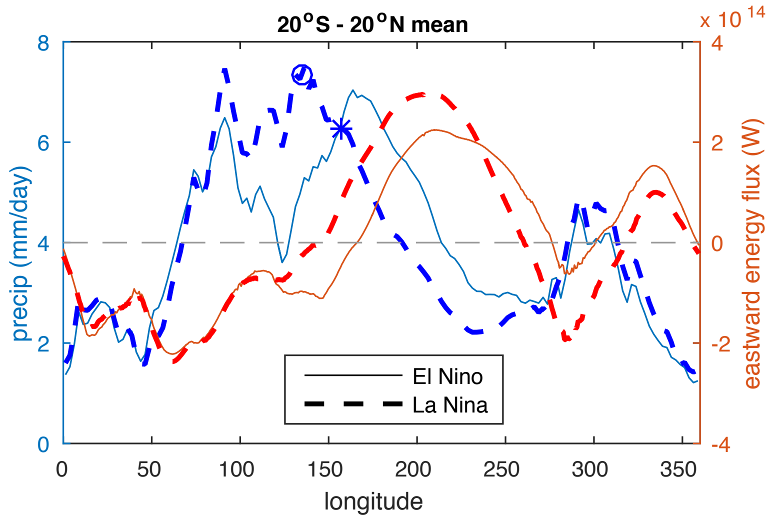

Supplementary Figure 1. **Same as Fig. 1b of main text, but for the entire tropics rather than a limited range of longitudes.**

E-mail addresses: billboos@alum.mit.edu.

DOI: 10.1038/NGEO2833

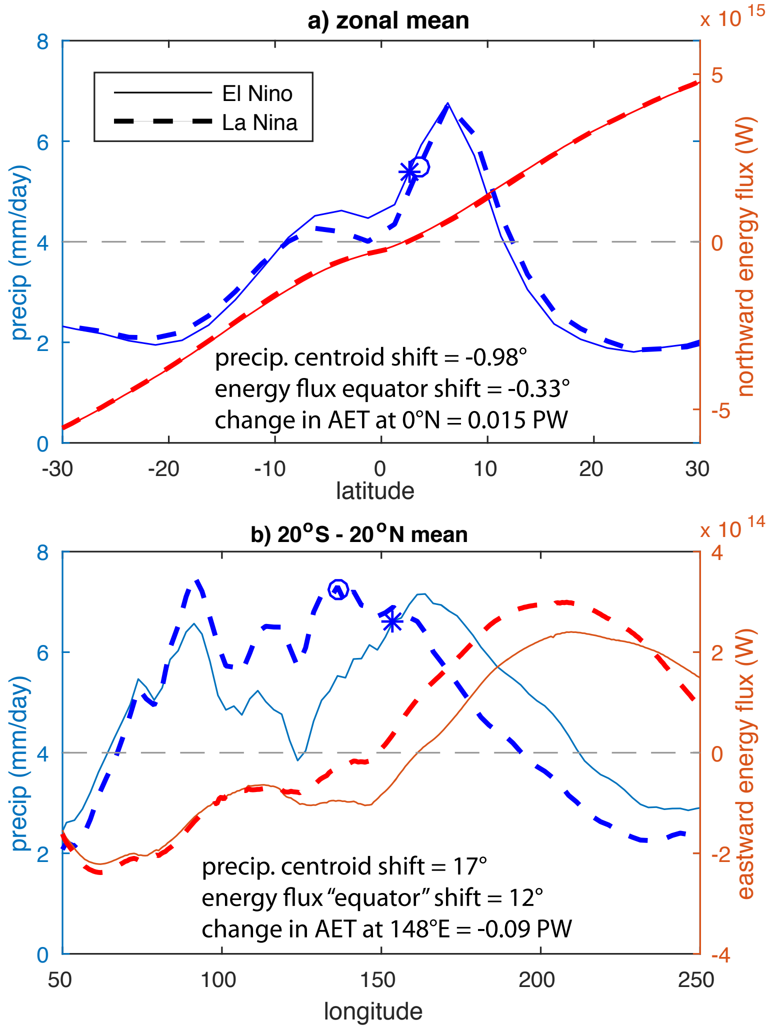

Supplementary Figure 2. **Same as Fig. 1 of main text, but with El Niño and La Niña states constructed using linear regression (rather than composite averaging).** Precipitation and AET are regressed on the NOAA ONI, then these regression coefficients are multiplied by one standard deviation of the ONI and added to the long-term climatological mean of each quantity to produce the El Niño state; the regression coefficients are multiplied by -1 in this procedure to produce the La Niña state.

1. Association of divergent energy fluxes with rainfall

The association between divergent winds and divergent AET is ensured for the zonal mean because nearly all zonal mean tropical AET is produced by the zonal mean meridional circulation, which by definition is purely divergent (i.e. irrotational). But at a particular longitude, the divergent AET could be nonzero even when the wind is exactly non-divergent, and in the tropics it is the time mean divergent wind that produces nearly all time mean rainfall[1]. In other words, in a zonally asymmetric climate, might rotational tropical winds balance a regional energy source through horizontal energy advection? Here we show that in one of the classic, idealized models for the zonally asymmetric circulation of Earth's tropical and subtropical troposphere, the divergent component of time mean winds produces most (i.e. more than half) of the vertically integrated energy flux divergence. This association between rainfall and the two-dimensional distribution of energy flux divergence in an idealized model motivates and helps justify the analyses conducted in the main text.

1.1. **Model details and methods.** We construct a fully nonlinear numerical version of the "Gill model", a canonical theoretical model for the atmospheric response to a zonally confined heat source[2]. When this heat source is positioned off the equator, previous solutions to the Gill model include many of the large-scale features of observed monsoons, with ascent near the heat source, subsidence to the west, and a zonal mean cross-equatorial Hadley circulation[3]. Here we construct a numerical version of the Gill model using version 5.1 of the Community Atmosphere Model (CAM5.1) produced by the National Center for Atmospheric Research. The original Gill model[2;3] lacked explicit moisture and imposed a diabatic heat source meant to represent a zonally confined precipitation maximum; since we wish to study energy transports in a moist, precipitating atmosphere we configure our model with a fully interactive hydrological cycle and an entirely oceanic surface (i.e. we run it in "aquaplanet" mode). A zonally confined, off-equatorial precipitation maximum is created by imposing a Gaussian sea surface temperature (SST) maximum centered at 25°N, 90°E — in roughly the location of the South Asian monsoon — on an otherwise globally uniform background SST of 300 K. The Gaussian SST anomaly has peak amplitude of 4 K and horizontal length scales (i.e. standard deviations) of 15° in longitude and 7.5° in latitude. The model is integrated using the finite volume dynamical core at 1.9°× 2.5° horizontal resolution in latitude and longitude, respectively, with 26 vertical levels. We used the subgrid scale physics from CAM4, including the Zhang-McFarlane deep convection scheme[4] and the Hack shallow convection scheme[5]. We prescribed an orbital eccentricity and obliquity of zero in the parameterizations for radiative transfer, thereby eliminating the seasonal cycle, but the details of radiative transfer have a relatively minor effect on solutions due to our use of prescribed SST.

Computation of the vertically integrated energy flux divergence is performed using data from the last nine years of a 10-year integration. We use the advective form of the energy equation, approximated as the time mean moist static energy budget,

$$\langle \mathbf{u} \cdot \nabla (c_p T + L_v q) \rangle + \left\langle \omega \frac{\partial h}{\partial p} \right\rangle = E + H + R \tag{1}$$

DOI: 10.1038/NGEO2833 SUPPLEMENTARY INFORMATION

where $\mathbf{u}$ is horizontal velocity, ω is vertical velocity, c_p is specific heat at constant pressure, T is temperature, L_v is the latent heat of vaporization, q is specific humidity, and E, H, and R are the net fluxes of latent heat, sensible heat, and radiative energy through the top and bottom boundaries of the atmosphere. Brackets denote a pressure-weighted vertical integral from surface pressure to the top of the model. The moist static energy $h = c_pT + L_vq + \Phi$ appears in the term representing vertical energy advection, but the geopotential Φ is omitted from the horizontal advection term, consistent with the primitive equations[6]; this form of the moist static energy equation has been used in other studies of tropical atmospheric dynamics[7]. The left side of equation (1) is equal to the divergence of the vertically integrated atmospheric energy flux, while the right side represents the column-integrated sources of moist static energy. We make all computations in the native model vertical coordinate (on η levels) and convert horizontal gradients to pressure coordinates via a standard transformation[8] for use in equation (1), although this coordinate transformation makes little difference since η and pressure surfaces are nearly parallel due to the lack of orography.

We calculate the vertically integrated atmospheric energy flux convergence accomplished by the total flow, by the time mean flow, and by transient anomalies to that time mean flow. First, we use 3-hourly samples of the model state to calculate each term on the left-hand side of equation (1), then average in time over 9 years. This is done only to confirm that the budget residual is acceptably small: its magnitude is 10% or less of the column-integrated energy source in the region of heavy rainfall. Our main task is using time mean values of T, q, h, $\mathbf{u}$, and ω to calculate the advective terms, which together give the atmospheric energy flux divergence produced by the time mean flow. After calculating the flux divergence produced by the total time mean flow, we decompose the time mean $\mathbf{u}$ into a horizontally divergent component $\mathbf{u}_\chi$ and a rotational component $\mathbf{u}_\psi$. These time mean divergent and rotational winds are then used with the time mean T, q, h, and ω in the left hand side of equation (1) to obtain the vertically integrated energy flux divergence produced by the time mean divergent flow and the time mean rotational flow. To be clear, the energy flux divergence by the time mean divergent wind consists of the sum of horizontal advection by the time mean divergent wind and vertical advection by the time mean flow, while energy flux divergence by the time mean rotational flow consists only of horizontal advection by the time mean rotational wind. The energy flux divergence by transients are computed as a residual by taking the right side of equation (1) and subtracting the energy flux divergence produced by the total time mean flow. Because our energy budget has a small residual, this yields a transient contribution similar to that obtained by explicit calculation from 3-hourly samples of the model state.

1.2. **Results.** Heavy rainfall (green contours in Supplementary Fig. 3a) occurs just south of the SST maximum, similar to the way that peak rainfall is centered just south of the maximum upper-tropospheric temperature and low-level moist static energy in observed monsoons[9]. This precipitation maximum is thus our idealized analogue of the regional rainfall maxima that occur in monsoon regions. There is strong subsidence and near zero precipitation west of the SST maximum, consistent with previous analytical and numerical solutions to the Gill model[2;3].

The total circulation diverges energy away from the precipitation maximum at a rate that peaks at about 600 W m^{-2} and is equal to the rate that energy is input to

DOI: 10.1038/NGEO2833

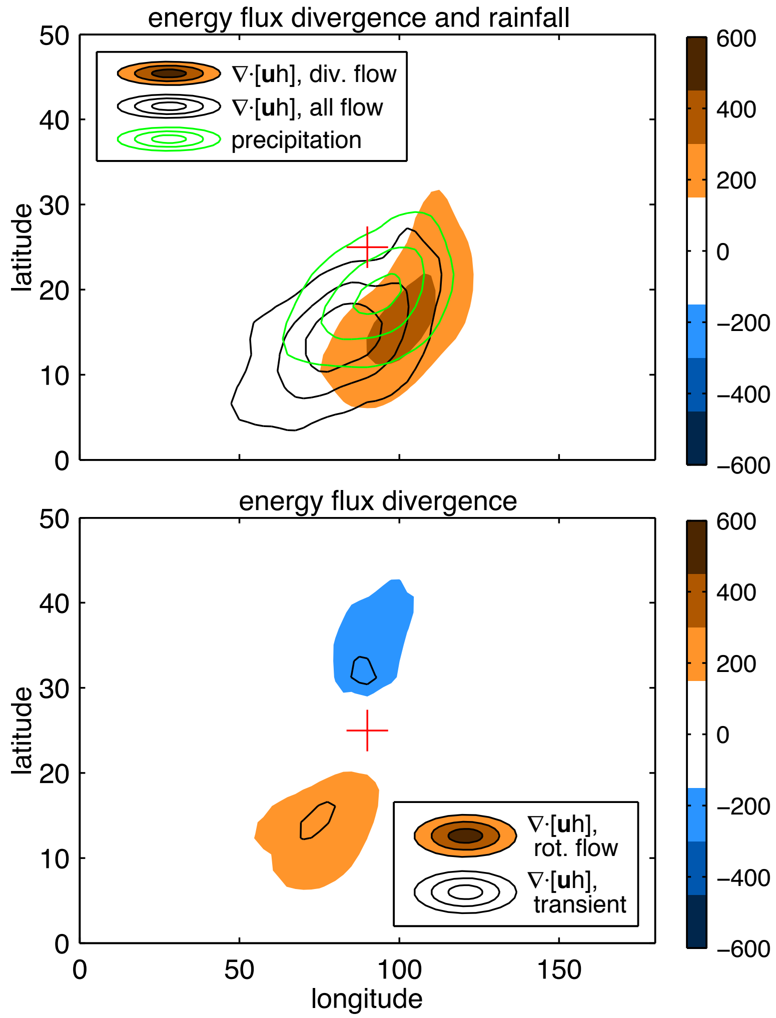

Supplementary Figure 3. **Association of rainfall with various components of the total atmospheric energy flux divergence in an idealized model.** a) time mean precipitation (green contours, interval 15 mm day^{-1} starting at 15 mm day^{-1}), total energy flux divergence (black contours), and the energy flux divergence produced by the time mean divergent wind (color shading). b) Energy flux divergence produced by the time mean rotational wind (color shading) and by transient motions (black contours). Red cross marks the center of the SST maximum and interval for all energy flux divergence contours is 150 W m^{-2}.

the atmosphere by surface enthalpy fluxes and radiation. The largest contribution to the total energy flux divergence generally comes from the divergent part of the time mean flow (compare black contours and color shading in Supplementary

DOI: 10.1038/NGEO2833

Fig. 3a). The rotational component of the time mean flow produces energy flux divergence with a peak magnitude of about one-third of the total, and the flux divergence produced by transients is even smaller (Supplementary Fig. 3b). There are regions where the rotational flow and transients together produce the majority of the total energy flux divergence, such as southwest of the SST maximum, but the contribution from the divergent wind can be seen to dominate in a bulk sense when one integrates over all regions of positive energy flux divergence (Supplementary Table 1).

This confirms that the divergent part of the time mean flow, which is associated with nearly all tropical and subtropical rainfall, produces the majority of the divergent AET, so one can indeed think of the regional ITCZ as being strongly associated with the regional vertically integrated energy flux divergence. It is possible that *perturbations* to the divergent AET will be dominated by perturbations in rotational flow or in transients that are not associated with time mean rainfall, but this is a subtlety that we leave for future work; results presented in the main text suggest that this is not the case for our mid-Holocene case study.

Supplementary Table 1. **Horizontally integrated positive atmospheric energy flux divergence in our numerical "Gill model".** The energy flux divergence produced by each of the listed wind components is horizontally integrated in a global domain over all regions where the flux divergence produced by that wind component is positive.

Component	Global integral
All winds	6.5 PW
Divergent time mean wind	6.2 PW
Rotational time mean wind	4.4 PW
Transient wind anomalies	3.2 PW

DOI: 10.1038/NGEO2833

Supplementary Table 2. **PMIP3 models analyzed and some of their characteristics.** "Type" indicates whether the model consists of coupled ocean-atmosphere (OA) components or coupled ocean-atmosphere-carbon cycle (OAC) components.

Model name	Atmospheric resolution (lat × lon × levels)	Type	Reference
CCSM4	0.9°× 1.25°× 26	OA	Gent et al. (2011)[10]
FGOALS-G2	2.8°× 2.8°× 26	OA	Li et al. (2013)[11]
MPI-ESM-P	1.9°× 1.9°× 25	OA	Giorgetta et al. (2013)[12]
MIROC-ESM	2.8°× 2.8°× 80	OAC	Sueyoshi et al. (2013)[13]

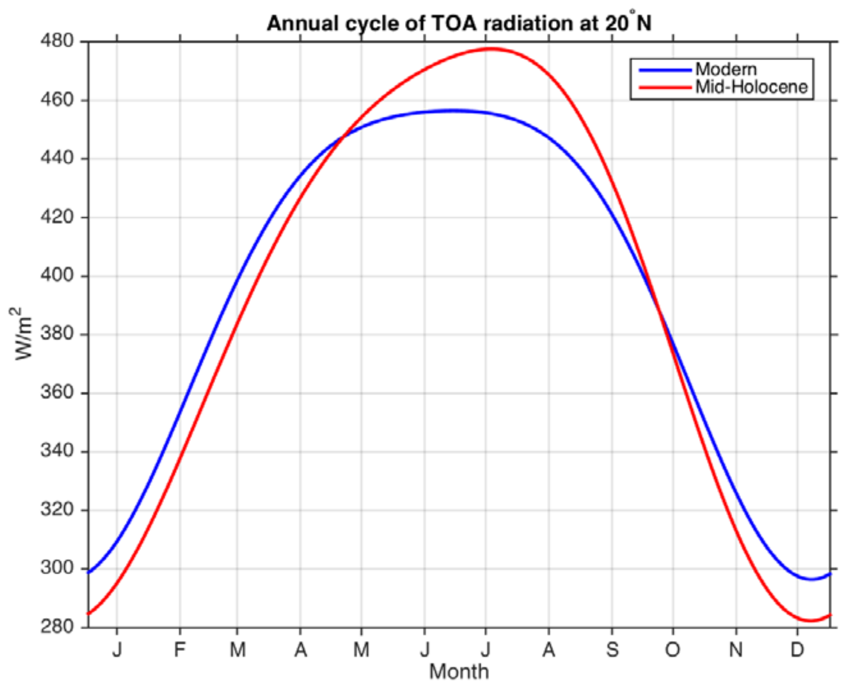

Supplementary Figure 4. Annual cycle of solar radiation incident at top of the atmosphere at 20°N during modern times (blue) and during the Mid-Holocene 6000 years ago (red). Grid lines are drawn at midpoint (15th day) of each month. Data from Berger 1978[14].

DOI: 10.1038/NGEO2833

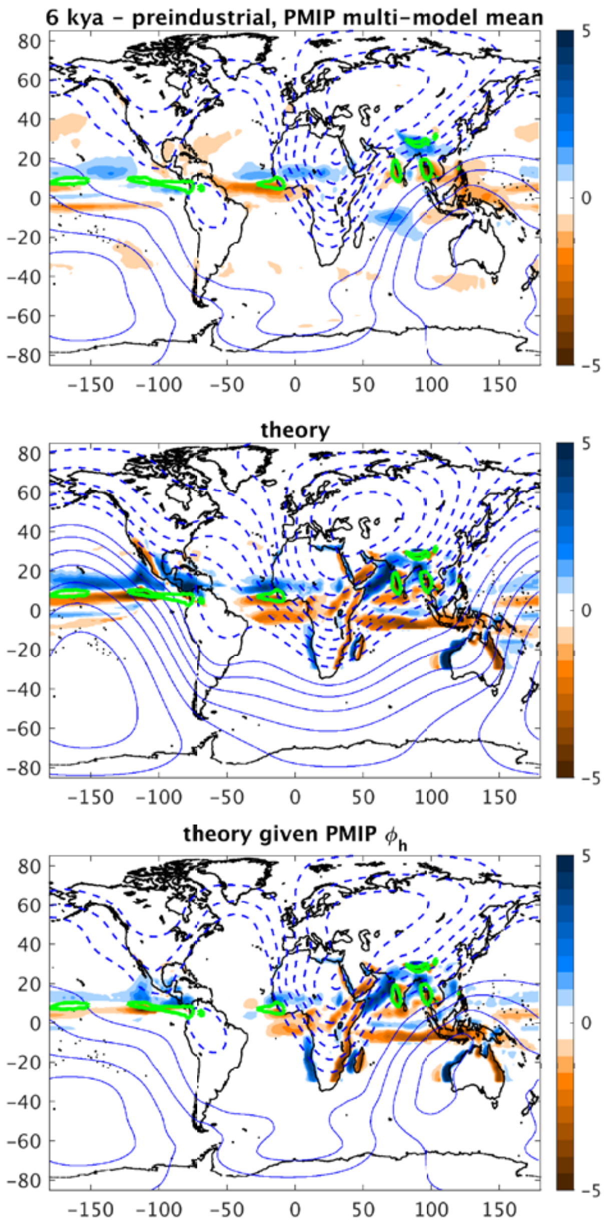

Supplementary Figure 5. **Same as left panels of Fig. 3 of main text but with color shading showing precipitation minus surface evapotranspiration ($P-E$) instead of preciptiation.** The green contour marks the 6 mm day^{-1} isoline of $P-E$.

DOI: 10.1038/NGEO2833

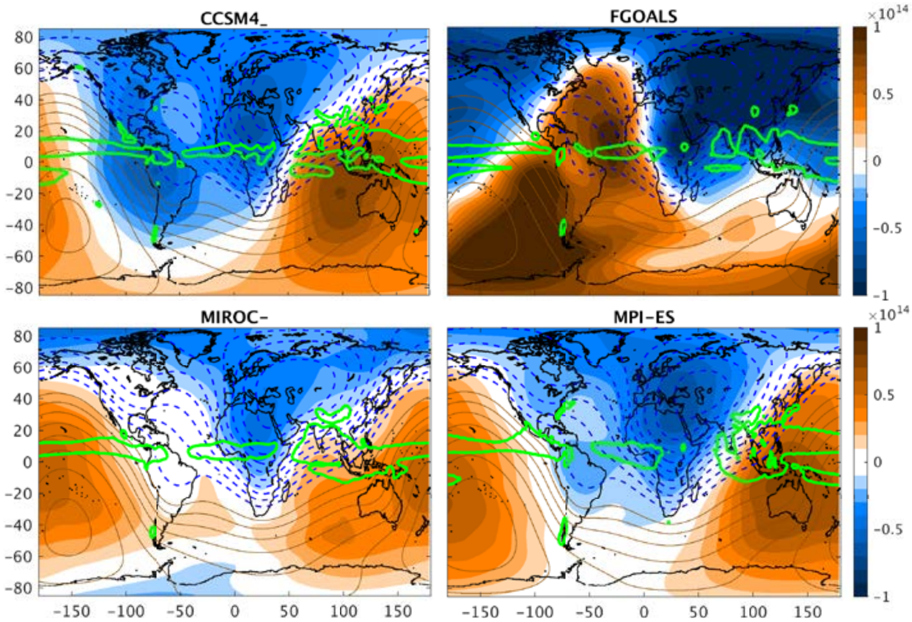

Supplementary Figure 6. **Energy flux potential response to mid-Holocene forcing in individual models.** Color shading shows the model-simulated anomalous energy flux potential and contours show the theoretical prediction of the anomalous energy flux potential, with all contour intervals 0.01 PW. Green contour marks the 6 mm day^{-1} isoline of precipitation. All quantities are May-Sept. climatological means.

References

[1] Seager, R. & Henderson, N. Diagnostic computation of moisture budgets in the ERA-interim reanalysis with reference to analysis of CMIP-archived atmospheric model data. *J. Clim.* **26**, 7876–7901 (2013).

[2] Gill, A. E. Some simple solutions for heat-induced tropical circulation. *Q. J. R. Meteorol. Soc.* **106**, 447–462 (1980).

[3] Rodwell, M. J. & Hoskins, B. J. Monsoons and the dynamics of deserts. *Q. J. R. Meteorol. Soc.* **122**, 1385–1404 (1996).

[4] Zhang, G. & McFarlane, N. A. Role of convective scale momentum transport in climate simulation. *J. Geophys. Res.* **100**, 1417–1426 (1995).

[5] Hack, J. J. Parameterization of moist convection in the National Center for Atmospheric Research community climate model (CCM2). *J. Geophys. Res.* **99**, 5551 (1994).

[6] Neelin, J. D. Moist dynamics of tropical convection zones in monsoons, teleconnections, and global warming. *Glob. Circ. Atmos.* 267–301 (2007).

[7] Sobel, A., Wang, S. & Kim, D. Moist static energy budget of the MJO during DYNAMO. *J. Atmos. Sci.* **71**, 4276–4291 (2014).

[8] Haltiner, G. J. & Williams, R. T. *Numerical prediction and dynamic meteorology*, vol. 2 (Wiley New York, 1980).

[9] Nie, J., Boos, W. R. & Kuang, Z. Observational evaluation of a convective quasi-equilibrium view of monsoons. *J. Clim.* **23**, 4416–4428 (2010).

[10] Gent, P. R. *et al.* The Community Climate System Model version 4. *J. Clim.* **24**, 4973–4991 (2011).

[11] Li, L. *et al.* The Flexible Global Ocean-Atmosphere-Land System model, grid-point version 2: FGOALS-g2. *Adv. Atmos. Sci.* **30**, 543–560 (2013).

[12] Giorgetta, M. A. *et al.* Climate and carbon cycle changes from 1850 to 2100 in MPI-ESM simulations for the coupled model intercomparison project phase 5. *J. Adv. Model. Earth Syst.* **5**, 572–597 (2013).

[13] Sueyoshi, T. *et al.* Set-up of the PMIP3 paleoclimate experiments conducted using an Earth system model, MIROC-ESM. *Geosci. Model Dev* **6**, 819–836 (2013).

[14] Berger, A. L. Long-term variations of caloric insolation from the Earth's orbital elements. *Quat. Res.* **9**, 139–167 (1978).